

# Vivim: a Video Vision Mamba for Medical Video Object Segmentation

Yijun Yang<sup>1</sup>, Zhaohu Xing<sup>1</sup>, and Lei Zhu<sup>1,2</sup>(✉)

<sup>1</sup> The Hong Kong University of Science and Technology (Guangzhou)  
yyang018@connect.hkust-gz.edu.cn

<sup>2</sup> The Hong Kong University of Science and Technology

**Abstract.** Traditional convolutional neural networks have a limited receptive field while transformer-based networks are mediocre in constructing long-term dependency from the perspective of computational complexity. Such the bottleneck poses a significant challenge when processing long video sequences in video analysis tasks. Very recently, the state space models (SSMs) with efficient hardware-aware designs, famous by Mamba, have exhibited impressive achievements in long sequence modeling, which facilitates the development of deep neural networks on many vision tasks. To better capture available cues in video frames, this paper presents a generic Video Vision Mamba-based framework for medical video object segmentation tasks, named **Vivim**. Our Vivim can effectively compress the long-term spatiotemporal representation into sequences at varying scales by our designed Temporal Mamba Block. Compared to existing video-level Transformer-based methods, our model maintains excellent segmentation results with better speed performance. Extensive experiments on breast lesion segmentation in ultrasound videos and polyp segmentation in colonoscopy videos demonstrate the effectiveness and efficiency of our Vivim. The code is available at: <https://github.com/scottyjyang/Vivim>.

**Keywords:** State space model · Mamba · Transformer · Video object segmentation.

## 1 Introduction

Automatic segmentation of lesions and tissues in medical videos is essential for computer-aided clinical examination and treatment [11], such as ultrasound breast lesion segmentation, polyp segmentation. Expanding the model’s receptive field in the spatiotemporal dimension is a critical aspect of advancing such video object segmentation tasks. Traditional convolutional neural networks [21,29,10,9] often struggle to capture global spatial information compared to recent transformer-based architectures. The transformer architecture, which utilizes the Multi-Head Self Attention (MSA) [23] to extract global information, has attracted much attention from the community of video object segmentation [28,1,19,17]. Considering that past frames offer a beneficial hint to the segmentation, these methods

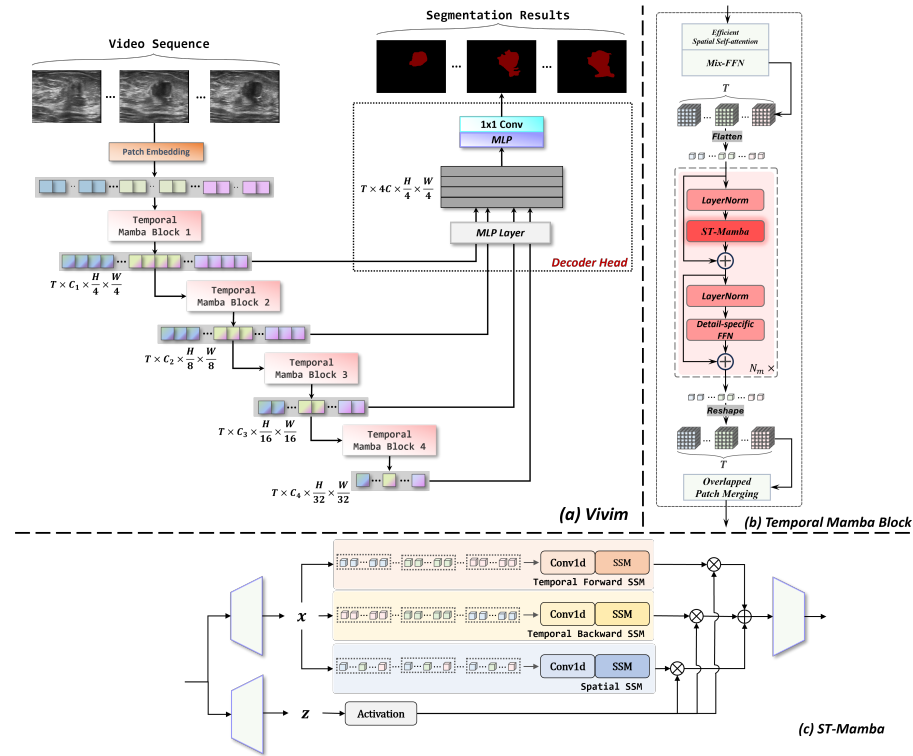


**Fig. 1.** (a) The overview of the proposed Vivim. (b) The fundamental building block of Vivim, namely Temporal Mamba Block. (c) ST-Mamba incorporates spatiotemporal sequence modeling for video vision tasks in a multi-way spirit.

usually introduce some elaborated modules to model the temporal information and integrate it with the spatial counterpart. However, the quadratic computation complexity impedes the application of the self-attention mechanism to video scenarios. The dramatically increasing number of tokens in long sequences from videos leads to significant computational burdens when adopting MSA for the simultaneous modeling of spatial and temporal information [1].

Very recently, to address the bottleneck concerning long sequence modeling, Mamba [8], inspired by state space models (SSMs) [15], has been developed. Its main idea is to effectively capture long-range dependencies and improve training and inference efficiency through the implementation of a selection scan mechanism and a hardware-aware algorithm. Based on this, U-Mamba [18] designed a hybrid CNN-SSM block, which is mainly composed of Mamba modules, to handle the long sequences in biomedical image segmentation tasks. Vision Mamba [30] provided a new generic vision backbone with bidirectional Mamba blocks on image classification and semantic segmentation tasks. As suggested by them, the reliance on the self-attention module is not necessary, and it can be easily replaced by Mamba to achieve efficient visual representation learning when com-

ing across long sequence modeling. Inherently, this offers an effective solution to explore long-term temporal dependency in video scenarios.

Inspired by this, we present a novel framework, named **Vivim**, that integrates Mamba into the multi-level transformer architecture to transform a video clip into one feature sequence containing spatiotemporal information at each scale. Our Vivim is designed to explore the temporal dependency across frames for the advancement of segmentation results with the cheaper computational cost than other video-based methods. To the best of our knowledge, this is the first work to incorporate Mamba into the task of video object segmentation, facilitating faster and greater performance. In our Vivim, drawing inspiration from the architecture of modern transformer blocks, we design a novel Temporal Mamba Block. A hierarchical encoder consisting of multiple Temporal Mamba Blocks is introduced to investigate the correlation between spatial and temporal dependency at various scales. As the structured state space sequence models with selective scan (S6) [8] causally process input data, they can only capture information within the scanned portion of the data. This aligns S6 with NLP and video tasks involving temporal data but poses challenges when addressing non-causal data like 2D images within medical videos. To this end, the structured state space sequence model with spatiotemporal selective scan, ST-Mamba, is incorporated into each scale of the model’s encoder, replacing the self-attention or window-attention module to achieve efficient visual representation learning. Finally, we leverage a lightweight CNN-based decoder head to integrate multi-level feature sequences and thus predict segmentation masks. We evaluate our framework Vivim on breast US videos and polyp colonoscopy videos. The experiments validate the universality and effectiveness of our method.

## 2 Method

In this part, we elaborate on a Mamba-based solution for video object segmentation tasks, named Vivim. Our Vivim mainly consists of two modules: A hierarchical encoder with the stacked Temporal Mamba Blocks to extract coarse and fine feature sequences at different scales, and a lightweight CNN-based decoder head to fuse multi-level feature sequences and predict segmentation masks. Fig. 1 (a) displays the flowchart of our proposed Vivim.

Given a video clip with  $T$  frames, *i.e.*,  $\mathbf{V} = \{I_1, \dots, I_T\}$ , we first divide these frames into patches of size  $4 \times 4$  by overlapped patch embedding. We then feed the sequence of patches into our hierarchical Temporal Mamba Encoder to obtain multi-level spatiotemporal features with resolution  $\{1/4, 1/8, 1/16, 1/32\}$  of the original frame. Finally, we pass multi-level features to the CNN-based decoder head to predict the segmentation results. Please refer to the following sections for more details about our proposed module.

### 2.1 Preliminaries

State Space Models (SSMs) are commonly considered as linear time-invariant systems, which map a 1-D function or sequence  $x(t) \in \mathbb{R} \mapsto y(t) \in \mathbb{R}$  through

a hidden state  $h(t) \in \mathbb{R}^N$ . This system is typically formulated as linear ordinary differential equations (ODEs), which uses  $\mathbf{A} \in \mathbb{R}^{N \times N}$  as the evolution parameter and  $\mathbf{B} \in \mathbb{R}^{N \times 1}$ ,  $\mathbf{C} \in \mathbb{R}^{1 \times N}$  as the projection parameters.

$$h'(t) = \mathbf{A}h(t) + \mathbf{B}x(t), \quad y(t) = \mathbf{C}h(t). \quad (1)$$

The discretization is introduced to primarily transform the ODE into a discrete function. This transformation is crucial to align the model with the sample rate of the underlying signal embodied in the input data, enabling computationally efficient operations. The structured state space sequence models (S4) and Mamba are the classical discrete versions of the continuous system, which include a timescale parameter  $\Delta$  to transform the continuous parameters  $\mathbf{A}$ ,  $\mathbf{B}$  to discrete parameters  $\bar{\mathbf{A}}$ ,  $\bar{\mathbf{B}}$ . The commonly used method for transformation is zero-order hold (ZOH), which is defined as follows:

$$\bar{\mathbf{A}} = \exp(\Delta \mathbf{A}), \quad \bar{\mathbf{B}} = (\Delta \mathbf{A})^{-1}(\exp(\Delta \mathbf{A}) - \mathbf{I}) \cdot \Delta \mathbf{B}. \quad (2)$$

After the discretization of  $\bar{\mathbf{A}}$ ,  $\bar{\mathbf{B}}$ , the discretized version of Eq. (1) can be rewritten as:

$$h_t = \bar{\mathbf{A}}h_{t-1} + \bar{\mathbf{B}}x_t, \quad y_t = \mathbf{C}h_t. \quad (3)$$

At last, the models compute output through a global convolution.

$$\bar{\mathbf{K}} = (\mathbf{C}\bar{\mathbf{B}}, \mathbf{C}\bar{\mathbf{A}}\bar{\mathbf{B}}, \dots, \mathbf{C}\bar{\mathbf{A}}^{M-1}\bar{\mathbf{B}}), \quad \mathbf{y} = \mathbf{x} * \bar{\mathbf{K}}, \quad (4)$$

where  $M$  is the length of the input sequence  $\mathbf{x}$ , and  $\bar{\mathbf{K}} \in \mathbb{R}^M$  is a structured convolutional kernel.

## 2.2 Overall architecture

**Hierarchical Feature Representation.** Multi-level features provide both high-resolution coarse features and low-resolution fine-grained features that significantly improve the segmentation results, especially for medical images. To this end, unlike Vivit [1], our encoder extracts multi-level multi-scale features given input video frames. Specifically, we perform patch merging frame-by-frame at the end of each Temporal Mamba Block, resulting in the  $i$ -th feature embedding  $\mathcal{F}_i$  with a resolution of  $\frac{H}{2^{i+1}} \times \frac{W}{2^{i+1}}$ .

**Temporal Mamba Block.** Exploring temporal information is critically important for video object segmentations by providing more object references. However, Multi-Head Self Attention (MSA) [23] in vanilla Transformer architectures has quadratic complexity concerning the number of tokens. This complexity is pertinent for long feature sequences from videos, as the number of tokens increases linearly with the number of input frames. Motivated by this, we develop a more efficient block, Temporal Mamba Block, to simultaneously model spatial and temporal information.

As illustrated in Fig. 1 (b), in the Temporal Mamba Block, an efficient spatial self-attention module is first introduced to provide the initial aggregation

of spatial information followed by a Mix-FeedForward layer. We leverage the sequence reduction process introduced in [26,24] to improve its efficiency. For the  $i$ -level feature embedding  $\mathcal{F}_i \in \mathbb{R}^{T \times C_i \times H \times W}$  of the given video clip, we first transpose the channel and temporal dimension, and employ a flattening operation to reshape the spatiotemporal feature embedding into 1D long sequence  $h_i \in \mathbb{R}^{C_i \times THW}$ , enabling highly efficient sequential modeling with less inductive bias. Then, the flattened sequence  $h_i$  is fed into layers of a Spatio-Temporal Mamba module (ST-Mamba) and a Detail-specific FeedForward (DSF). The ST-Mamba module establishes the intra- and inter-frame long-range dependencies while the Detail-specific Feedforward preserves fine-grained details by a depth-wise convolution with a kernel size of  $3 \times 3 \times 3$ . After the DSF, the feature is returned to the original shape by its inverse operation. Finally, we employ overlapped patch merging to down-sampling the feature embedding. The procedure in the Mamba Layer can be defined as:

$$\begin{aligned}
 h^{l-1} &= \phi(h^{l-1}), \\
 \hat{h}^l &= \text{ST-Mamba}(\text{LayerNorm}(h^{l-1})) + h^{l-1}, \\
 h^l &= \text{DSF}(\text{LayerNorm}(\hat{h}^l)) + \hat{h}^l, \\
 h^l &= \phi^{-1}(h^l),
 \end{aligned} \tag{5}$$

where  $\phi$  denotes the transposition and flattening operation,  $\phi^{-1}$  denotes its inverse operation,  $l \in [1, N_m]$ .

**Decoder.** To predict the segmentation mask from the multi-level feature embeddings, we introduce a CNN-based decoder head following [26]. While our hierarchical Temporal Mamba encoder has a large effective receptive field across spatial and temporal axes, the CNN-based decoder head further refines the details of local regions. To be specific, the multi-level features  $\{\mathcal{F}_1, \mathcal{F}_2, \mathcal{F}_3, \mathcal{F}_4\}$  from the temporal mamba blocks are passed into an MLP layer to unify the channel dimension. These unified features are up-sampled to the same resolution and concatenated together. Third, a MLP layer is adopted to fuse the concatenated features  $\mathcal{F}$ . Finally, The fused feature goes through a  $1 \times 1$  convolutional layer to predict the segmentation mask  $\mathcal{M}$ .

### 2.3 Spatiotemporal Selective Scan

Despite the causal nature of S6 for temporal data, videos differ from texts in that they not only contain temporal redundant information but also accumulate 2D spatial information as the non-causal images do. To address this problem, we introduce ST-Mamba, which incorporates spatiotemporal sequence modeling for video vision tasks, as displayed in Fig. 1 (c).

Specifically, to explicitly explore the relationship among frames, we first unfold patches of each frame along rows and columns into sequences, and then concatenate the frame sequences to constitute the video sequence  $h_i^t \in \mathbb{R}^{C_i \times T(HW)}$ . We parallelly proceed with scanning along the forward and backward directions

to explore bidirectional temporal dependency. This approach allows the models to compensate for each other’s receptive fields without significantly increasing computational complexity. Simultaneously, we stack patches along the temporal axis and construct the spatial sequence  $h_i^s \in \mathbb{R}^{C_i \times (HW)^T}$ . We proceed with scanning to integrate information of each pixel from all frames. The spatiotemporal selective scan explicitly considers both single-frame spatial coherence and cross-frame coherence, and leverages parallel SSMs to establish the intra- and inter-frame long-range dependencies, resulting in more effective visual representation learning. The structured state space sequence models with spatiotemporal selective scan (ST-Mamba), serve as the core element to construct the Temporal Mamba block, which constitutes the fundamental building block of Vivim.

**Computational-Efficiency.** SSMs in ST-Mamba and self-attention in Transformer both provide a crucial solution to model spatiotemporal context adaptively. Given a video visual sequence  $\mathbf{F} \in \mathbb{R}^{1 \times T \times M \times D}$ , the computation complexity of a global self-attention and SSM are:

$$\Omega(\text{self-attention}) = 4(\text{TM})D^2 + 2(\text{TM})^2D, \quad (6)$$

$$\Omega(\text{SSM}) = 4(\text{TM})(2D)N + (\text{TM})(2D)N^2, \quad (7)$$

where the default expansion ratio is 2,  $N$  is a fixed parameter and set to 16. As observed, self-attention is quadratic to the whole video sequence length ( $\text{TM}$ ), and SSM is linear to that. Such computational efficiency makes ST-Mamba a better solution for long-term video applications.

## 3 Experiments

### 3.1 Dataset and Implementation

We evaluate our Vivim on two popular medical video object segmentation tasks, *i.e.*, video polyp segmentation and video breast lesion segmentation. Specifically, for video polyp segmentation, we adopt four widely used polyp datasets, including image-based Kvasir [12] and video-based CVC-300 [3], CVC-612 [2] and ASU-Mayo [22]. Following the same protocol as [14], we train our model on Kvasir, ASU-Mayo and the training sets of CVC-300 and CVC-612, and conduct three experiments on test datasets CVC-300-TV, CVC-612-V and CVC-612-T. For video breast lesion segmentation, we conduct experiments on the breast ultrasound (US) dataset [16] consisting of 63 video sequences, with one video sequence per person, containing 4619 frames that have been annotated with pixel-level ground truth by experts. Following the approach outlined in [16], the video sequences with spatial resolutions ranging from  $580 \times 600$  to  $600 \times 800$  were further cropped to a spatial resolution of  $300 \times 200$ . We follow the official splits for training and testing.

The proposed framework was trained on one NVIDIA RTX 3090 GPU and implemented on the Pytorch platform. Our framework is empirically trained for 100 epochs in an end-to-end way and the Adam optimizer is applied. The initial learning rate is set to  $1 \times 10^{-4}$  and decayed to  $1 \times 10^{-6}$ . During training, we

**Table 1.** Quantitative results on different datasets. The best scores are highlighted in bold.  $\uparrow$  indicates the higher the score the better, and vice versa.

Metrics	2018~2019			2020~2021			2024	
	UNet MICCAI [21]	UNet++ TMI [29]	ResUNet ISM [13]	ACSNet MICCAI [27]	PraNet MICCAI [7]	PNS-Net MICCAI [14]	<b>Vivim (Ours)</b>	
CVC-300-TV	maxDice $\uparrow$	0.639	0.649	0.535	0.738	0.739	0.840	<b>0.880</b>
	maxSpe $\uparrow$	0.963	0.944	0.852	0.987	0.993	<b>0.996</b>	0.991
	maxIoU $\uparrow$	0.525	0.539	0.412	0.632	0.645	0.745	<b>0.807</b>
	$S_\alpha \uparrow$	0.793	0.796	0.703	0.837	0.833	0.909	<b>0.928</b>
	$E_\phi \uparrow$	0.826	0.831	0.718	0.871	0.852	0.921	<b>0.959</b>
	MAE $\downarrow$	0.027	0.024	0.052	0.016	0.016	0.013	<b>0.008</b>
	CVC-612-V	maxDice $\uparrow$	0.725	0.684	0.752	0.804	0.869	0.873
maxSpe $\uparrow$		0.971	0.952	0.939	0.929	0.983	0.991	<b>0.992</b>
maxIoU $\uparrow$		0.610	0.570	0.648	0.712	0.799	0.800	<b>0.822</b>
$S_\alpha \uparrow$		0.826	0.805	0.829	0.847	0.915	0.923	<b>0.943</b>
$E_\phi \uparrow$		0.855	0.830	0.877	0.887	0.936	0.944	<b>0.976</b>
MAE $\downarrow$		0.023	0.025	0.023	0.054	0.013	0.012	<b>0.009</b>
CVC-612-T		maxDice $\uparrow$	0.729	0.740	0.617	0.782	0.852	0.860
	maxSpe $\uparrow$	0.971	0.975	0.950	0.975	0.986	0.992	<b>0.992</b>
	maxIoU $\uparrow$	0.635	0.635	0.514	0.700	0.786	0.795	<b>0.809</b>
	$S_\alpha \uparrow$	0.810	0.800	0.727	0.838	0.886	0.903	<b>0.917</b>
	$E_\phi \uparrow$	0.836	0.817	0.758	0.864	0.904	0.903	<b>0.924</b>
	MAE $\downarrow$	0.058	0.059	0.084	0.053	0.038	0.038	<b>0.033</b>

**Table 2.** Quantitative comparison with different methods on breast US dataset.

Methods	Jaccard $\uparrow$	Dice $\uparrow$	Precision $\uparrow$	Recall $\uparrow$	FPS $\uparrow$
UNet [21]	62.47 $\pm$ 0.53	73.03 $\pm$ 0.36	79.46 $\pm$ 0.20	72.72 $\pm$ 0.45	88.18
UNet++ [29]	61.24 $\pm$ 0.73	71.79 $\pm$ 0.53	82.80 $\pm$ 0.04	68.84 $\pm$ 1.09	40.9
TransUNet [4]	53.58 $\pm$ 0.37	65.47 $\pm$ 0.21	71.67 $\pm$ 0.13	66.82 $\pm$ 0.20	65.1
SETR [28]	54.80 $\pm$ 0.68	66.49 $\pm$ 0.59	75.33 $\pm$ 0.15	66.43 $\pm$ 1.04	21.61
OSVOS [20]	56.74 $\pm$ 0.59	70.98 $\pm$ 0.33	77.78 $\pm$ 0.92	64.04 $\pm$ 0.98	27.25
ViViT [1]	54.46 $\pm$ 0.32	67.39 $\pm$ 0.29	75.54 $\pm$ 0.03	66.83 $\pm$ 0.59	24.33
STM [19]	68.58 $\pm$ 0.56	78.62 $\pm$ 0.43	82.01 $\pm$ 0.35	79.10 $\pm$ 0.44	23.17
AFB-URR [17]	70.34 $\pm$ 0.25	80.18 $\pm$ 0.15	80.08 $\pm$ 0.32	85.91 $\pm$ 0.15	11.84
DPSTT [16]	73.64 $\pm$ 0.18	82.55 $\pm$ 0.20	83.89 $\pm$ 0.13	84.55 $\pm$ 0.29	30.5
Ours	<b>73.94</b>	<b>83.22</b>	<b>84.34</b>	<b>86.44</b>	<b>35.33</b>

resize the video frames to  $256 \times 256$ , and feed a batch of 8 video clips, each of which has 5 frames, into the network for each iteration. We use cross-entropy loss and IoU loss as the objective function of our method.

### 3.2 Evaluation on video polyp segmentation

**Metrics.** We adopt six metrics following [14], *i.e.*, maximum Dice (maxDice), maximum specificity (maxSpe), maximum IoU (maxIoU), S-measure [5] ( $S_\alpha$ ), enhanced-alignment measure [6] ( $E_\phi$ ), and mean absolute error (MAE).

**Quantitative comparison.** we compare our method with many state-of-the-art methods as summarized in Tab. 1, including UNet [21], UNet++ [29], ResUNet [13], ACSNet [27], PraNet [7] and PNS-Net [14]. We conduct three experiments on test datasets of CVC-300 and CVC-612 to validate the model’s performance. CVC-300-TV consists of both validation set and test set, which

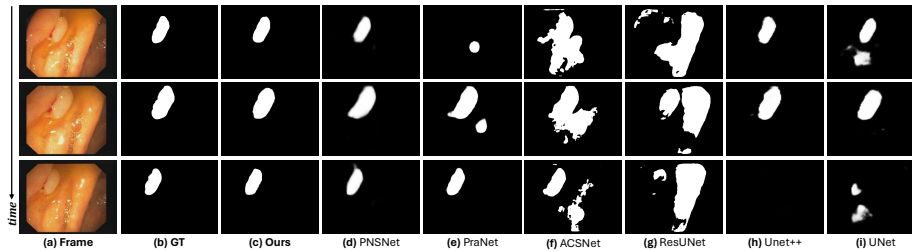


**Fig. 2.** Qualitative results on CVC-612-T.

include six videos in total. CVC-612-V and CVC-612-T each contain five videos. On CVC-300-TV, our Vivim achieves remarkable performance and outperforms all SOTA methods by a large margin across most metrics (*e.g.*, 4.0% in maxDice, 6.2% in maxIoU). On CVC-612-V and CVC-612-T, our Vivim consistently outperforms other SOTAs, especially 2.2% and 1.0% in maxDice, respectively.

**Qualitative comparison.** In Fig. 2, we visualize the polyp segmentation results of our Vivim on the consecutive frames of CVC-612-T. Our model can better locate and segment polyps with more accurate boundaries.

### 3.3 Evaluation on US video breast lesion segmentation

**Metrics.** We utilized several commonly employed segmentation evaluation metrics, including the Jaccard similarity coefficient (Jaccard), Dice similarity coefficient (Dice), Precision, and Recall; for their precise definitions, please refer to [25]. We also report the inference speed performance of different methods by computing the number of frames per second (FPS).

**Quantitative comparison.** As shown in Tab. 2, we quantitatively compare our method with many state-of-the-art methods on breast US videos dataset. These methods including popular medical image segmentation methods (UNet [21], UNet++ [29], TransUNet [4]), image segmentation method SERT [28] and video object segmentation methods (OSVOS [20], ViViT [1], STM [19], AFB-URR [17], DPSTT [16]). For the fairness of comparisons, we reproduce these methods using their publicly available codes following [16]. We can observe that video-based methods tend to outperform image-based methods as evidenced by their better performance. This suggests that the exploration of temporal information offers significant advantages for segmenting breast lesions in ultrasound videos. More importantly, among all image-based and video-based segmentation methods, our Vivim has achieved the highest performance across all scores. In particular, our Vivim has the best run-time among all video-based methods observed from the evaluation on FPS. This demonstrates that our solution can simultaneously learn spatial and temporal cues in an efficient way, and achieves significant improvements over those Transformer methods, such as SERT and ViViT.

## 4 Conclusion

In this paper, we present a Mamba-based framework Vivim to address the challenges in modeling long-range temporal dependencies due to the inherent locality of CNNs and the high computational complexity of Transformers. The main idea of Vivim is to introduce the structured state space models with spatiotemporal selective scan, ST-Mamba, into the standard hierarchical Transformer architecture. This facilitates the exploration of spatiotemporal information in a computationally cheaper way than using the self-attention mechanism. Experimental results on polyp colonoscopy videos and breast US videos reveal that Vivim outperforms existing image- and video-level segmentation networks. More importantly, Vivim has superior capabilities in handling long video sequences with lower computational costs compared to Vivit. In the further, We will apply our solution to more video object segmentation tasks.

## References

1. Arnab, A., Dehghani, M., Heigold, G., Sun, C., Lučić, M., Schmid, C.: Vivit: A video vision transformer. In: Proceedings of the IEEE/CVF international conference on computer vision. pp. 6836–6846 (2021)
2. Bernal, J., Sánchez, F.J., Fernández-Esparrach, G., Gil, D., Rodríguez, C., Vilarino, F.: Wm-dova maps for accurate polyp highlighting in colonoscopy: Validation vs. saliency maps from physicians. *Computerized medical imaging and graphics* **43**, 99–111 (2015)
3. Bernal, J., Sánchez, J., Vilarino, F.: Towards automatic polyp detection with a polyp appearance model. *Pattern Recognition* **45**(9), 3166–3182 (2012)
4. Chen, J., Lu, Y., Yu, Q., Luo, X., Adeli, E., Wang, Y., Lu, L., Yuille, A.L., Zhou, Y.: Transunet: Transformers make strong encoders for medical image segmentation. arXiv preprint arXiv:2102.04306 (2021)
5. Fan, D.P., Cheng, M.M., Liu, Y., Li, T., Borji, A.: Structure-measure: A new way to evaluate foreground maps. In: Proceedings of the IEEE international conference on computer vision. pp. 4548–4557 (2017)
6. Fan, D.P., Ji, G.P., Qin, X., Cheng, M.M.: Cognitive vision inspired object segmentation metric and loss function. *Scientia Sinica Informationis* **6**(6) (2021)
7. Fan, D.P., Ji, G.P., Zhou, T., Chen, G., Fu, H., Shen, J., Shao, L.: Pranel: Parallel reverse attention network for polyp segmentation. In: International conference on medical image computing and computer-assisted intervention. pp. 263–273. Springer (2020)
8. Gu, A., Dao, T.: Mamba: Linear-time sequence modeling with selective state spaces. arXiv preprint arXiv:2312.00752 (2023)
9. He, K., Gkioxari, G., Dollár, P., Girshick, R.: Mask r-cnn. In: Proceedings of the IEEE international conference on computer vision. pp. 2961–2969 (2017)
10. He, K., Zhang, X., Ren, S., Sun, J.: Deep residual learning for image recognition. In: Proceedings of the IEEE conference on computer vision and pattern recognition. pp. 770–778 (2016)
11. Huang, Q., Huang, Y., Luo, Y., Yuan, F., Li, X.: Segmentation of breast ultrasound image with semantic classification of superpixels. *Medical Image Analysis* **61**, 101657 (2020)

12. Jha, D., Smedsrud, P.H., Riegler, M.A., Halvorsen, P., de Lange, T., Johansen, D., Johansen, H.D.: Kvasir-seg: A segmented polyp dataset. In: *MultiMedia Modeling: 26th International Conference, MMM 2020, Daejeon, South Korea, January 5–8, 2020, Proceedings, Part II* 26. pp. 451–462. Springer (2020)
13. Jha, D., Smedsrud, P.H., Riegler, M.A., Johansen, D., De Lange, T., Halvorsen, P., Johansen, H.D.: Resunet++: An advanced architecture for medical image segmentation. In: *2019 IEEE international symposium on multimedia (ISM)*. pp. 225–2255. IEEE (2019)
14. Ji, G.P., Chou, Y.C., Fan, D.P., Chen, G., Fu, H., Jha, D., Shao, L.: Progressively normalized self-attention network for video polyp segmentation. In: *International Conference on Medical Image Computing and Computer-Assisted Intervention*. pp. 142–152. Springer (2021)
15. Kalman, R.E.: A new approach to linear filtering and prediction problems (1960)
16. Li, J., Zheng, Q., Li, M., Liu, P., Wang, Q., Sun, L., Zhu, L.: Rethinking breast lesion segmentation in ultrasound: A new video dataset and a baseline network. In: *International Conference on Medical Image Computing and Computer-Assisted Intervention*. pp. 391–400. Springer (2022)
17. Liang, Y., Li, X., Jafari, N., Chen, J.: Video object segmentation with adaptive feature bank and uncertain-region refinement. *Advances in Neural Information Processing Systems* **33**, 3430–3441 (2020)
18. Ma, J., Li, F., Wang, B.: U-mamba: Enhancing long-range dependency for biomedical image segmentation. *arXiv preprint arXiv:2401.04722* (2024)
19. Oh, S.W., Lee, J.Y., Xu, N., Kim, S.J.: Video object segmentation using space-time memory networks. In: *Proceedings of the IEEE/CVF International Conference on Computer Vision*. pp. 9226–9235 (2019)
20. Perazzi, F., Khoreva, A., Benenson, R., Schiele, B., Sorkine-Hornung, A.: Learning video object segmentation from static images. In: *Proceedings of the IEEE conference on computer vision and pattern recognition*. pp. 2663–2672 (2017)
21. Ronneberger, O., Fischer, P., Brox, T.: U-net: Convolutional networks for biomedical image segmentation. In: *International Conference on Medical Image Computing and Computer-Assisted Intervention*. pp. 234–241. Springer (2015)
22. Tajbakhsh, N., Gurudu, S.R., Liang, J.: Automated polyp detection in colonoscopy videos using shape and context information. *IEEE transactions on medical imaging* **35**(2), 630–644 (2015)
23. Vaswani, A., Shazeer, N., Parmar, N., Uszkoreit, J., Jones, L., Gomez, A.N., Kaiser, Ł., Polosukhin, I.: Attention is all you need. *Advances in neural information processing systems* **30** (2017)
24. Wang, W., Xie, E., Li, X., Fan, D.P., Song, K., Liang, D., Lu, T., Luo, P., Shao, L.: Pyramid vision transformer: A versatile backbone for dense prediction without convolutions. In: *Proceedings of the IEEE/CVF international conference on computer vision*. pp. 568–578 (2021)
25. Wang, Y., Deng, Z., Hu, X., Zhu, L., Yang, X., Xu, X., Heng, P.A., Ni, D.: Deep attentional features for prostate segmentation in ultrasound. In: *Medical Image Computing and Computer Assisted Intervention–MICCAI 2018: 21st International Conference, Granada, Spain, September 16–20, 2018, Proceedings, Part IV* 11. pp. 523–530. Springer (2018)
26. Xie, E., Wang, W., Yu, Z., Anandkumar, A., Alvarez, J.M., Luo, P.: Segformer: Simple and efficient design for semantic segmentation with transformers. *Advances in Neural Information Processing Systems* **34**, 12077–12090 (2021)

27. Zhang, R., Li, G., Li, Z., Cui, S., Qian, D., Yu, Y.: Adaptive context selection for polyp segmentation. In: Medical Image Computing and Computer Assisted Intervention–MICCAI 2020: 23rd International Conference, Lima, Peru, October 4–8, 2020, Proceedings, Part VI 23. pp. 253–262. Springer (2020)
28. Zheng, S., Lu, J., Zhao, H., Zhu, X., Luo, Z., Wang, Y., Fu, Y., Feng, J., Xiang, T., Torr, P.H., et al.: Rethinking semantic segmentation from a sequence-to-sequence perspective with transformers. In: Proceedings of the IEEE/CVF conference on computer vision and pattern recognition. pp. 6881–6890 (2021)
29. Zhou, Z., Rahman Siddiquee, M.M., Tajbakhsh, N., Liang, J.: Unet++: A nested u-net architecture for medical image segmentation. In: Deep learning in medical image analysis and multimodal learning for clinical decision support, pp. 3–11. Springer (2018)
30. Zhu, L., Liao, B., Zhang, Q., Wang, X., Liu, W., Wang, X.: Vision mamba: Efficient visual representation learning with bidirectional state space model. arXiv preprint arXiv:2401.09417 (2024)